Available online at www.sciencedirect.com
SCIENCE DIRECT®
Journal of Molecular Catalysis A: Chemical 209 (2004) 145–153
JOURNAL OF MOLECULAR CATALYSIS A: CHEMICAL
www.elsevier.com/locate/molcata

Mechanistic study on skeletal isomerization of *n*-butane using 1,4-$^{13}C_2$-*n*-butane on typical solid acids and their Pt-promoted bifunctional catalysts

Tsuneo Echizen [a], Tetsuo Suzuki [a], Yuichi Kamiya [b], Toshio Okuhara [a,*]

[a] *Graduate School of Environmental Earth Science, Hokkaido University, Sapporo 060-0810, Japan*
[b] *Japan Science and Technology Corporation, 4-1-8 Honcho, Kawagachi 332-0012, Japan*

Received 17 June 2003; received in revised form 28 July 2003; accepted 18 August 2003

Abstract

The reaction mechanism of skeletal isomerization of *n*-butane over typical solid acids such as $Cs_{2.5}H_{0.5}PW_{12}O_{40}$, sulfated ZrO_2, and WO_3/ZrO_2 and their Pt-promoted catalysts have been studied by the use of 1,4-$^{13}C_2$-*n*-butane. Isotopic distributions in product isobutane and reactant *n*-butane were quantitatively analyzed by field-ionization mass spectrometry (FI-MS). On these solid acids, below 423 K, isobutane consisted of $^{13}C_0$–$^{13}C_4$ isotopes, whose distributions were close to the corresponding binomial distributions, with the reactant *n*-butane being mainly $^{13}C_2$-*n*-butane. This indicates that the isomerization proceeded with an intermolecular rearrangement through a bimolecular mechanism. In the temperature range of 493–523 K over these solid acids, the isotopic distributions in isobutane deviated from the binomial distributions; the fractions of $^{13}C_2$-isobutane were greater than those expected from the binomial distributions, showing that an intramolecular (monomolecular) rearrangement became significant. Further, the product isobutane was found to consist of exclusively $^{13}C_2$-isobutane over these Pt-promoted catalysts in the presence of H_2, demonstrating the operation of a monomolecular mechanism on the bifunctional catalysts.

Keywords: Isomerization of *n*-butane; Reaction mechanism; 1,4-^{13}C-*n*-butane; Solid acid; Bifunctional catalyst; Field-ionization mass spectrometry

1. Introduction

Skeletal isomerization of *n*-butane is of practical importance because the product isobutane is the main intermediate for alkylation with butenes to form clean high-octane gasoline (C_8-branched alkanes). The reaction of *n*-butane is thus of particular interest, although among *n*-alkanes, *n*-butane is much less reactive for the skeletal isomerization. Many reports on this reaction have been published. Liquid acids such as HF are active [1,2], but these have problems of high toxicity, catalyst waste, use of large amounts of catalyst, and difficulty in separation and recovery. Solid acids are environmentally benign, because the above problems are eliminated. The solid acids are required to have high acid strength because of the low reactivity of *n*-butane. Sulfated zirconia (SO_4^{2-}/ZrO_2) catalyzes this reaction at low temperatures [3–5]. In addition, an acidic Cs salt of 12-tungstophosphoric acid, $Cs_{2.5}H_{0.5}PW_{12}O_{40}$, selectively catalyzes the isomerization of *n*-butane even at 573 K [6,7]. WO_3/ZrO_2 was reported to be active for the reaction [8,9].

Besides these solid acids, noble metal, such as Pt-promoted solid acids are promising catalysts in the presence of H_2. Pt-SO_4^{2-}/ZrO_2 is highly active for the isomerization of *n*-butane [10,11] and has been utilized as a commercial catalyst for isomerization of C_5 and C_6 hydrocarbons [12]. Pt-$Cs_{2.5}H_{0.5}PW_{12}O_{40}$ was reported to be highly selective (>95%) in the presence of H_2 [13,14]. Pt-WO_3/ZrO_2 also showed a high selectivity for isomerization of *n*-butane, although the activity is not high [15,16].

Since the selectivity to isobutane in the isomerization of *n*-butane is closely related to the reaction mechanism, understanding the mechanism is indispensable for development of appropriate catalysts. It is generally accepted that this reaction occurs through two possible pathways: a monomolecular pathway with intramolecular rearrangement, and a bimolecular pathway accompanying intermolecular rearrangement [17]. One of the promising approaches for elucidation of the reaction mechanism is utilization of

* Corresponding author. Tel.: +81-11-706-4513; fax: +81-11-706-4513.
E-mail address: oku@ees.hokudai.ac.jp (T. Okuhara).

1381-1169/$ – see front matter © 2003 Elsevier B.V. All rights reserved.
doi:10.1016/j.molcata.2003.08.021

^{13}C-labeled butanes as reactants. Analysis of the isotopic distributions of the product butanes and the location of ^{13}C in the butanes gives helpful information on the reaction mechanism. Thus far, mechanistic studies on the *n*-butane isomerization have been done over SO_4^{2-}/ZrO_2 [18,19] and H-mordenite [20] using ^{13}C-labeled butanes. However, the results are contradictory, and the mechanism remains a point of controversy.

According to Grain et al. [18], this reaction occurs through the monomolecular mechanism at 523 K over SO_4^{2-}/ZrO_2 and Pt-SO_4^{2-}/ZrO_2. In contrast, Adeeva et al. [19] have implied that it proceeds through the bimolecular mechanism at 353 K over SO_4^{2-}/ZrO_2. Matsuhashi et al. [21] presumed that over SO_4^{2-}/ZrO_2, the monomolecular mechanism dominates at the initial stage of reaction and the bimolecular mechanism dominates at the latter stage. We preliminarily reported that over $Cs_{2.5}H_{0.5}PW_{12}O_{40}$, this reaction takes place in a parallel manner via both monomolecular and bimolecular mechanisms [22], and that the monomolecular mechanism mainly operates for Pt-$Cs_{2.5}H_{0.5}PW_{12}O_{40}$ [23].

In the present study, we attempted to systematically study the mechanism with typical solid acids and the Pt-promoted catalysts by using 1,4-$^{13}C_2$-*n*-butane. We wish to emphasize that the isotopic composition was analyzed by field-ionization mass spectrometry (FI-MS). FI-MS is a "soft" ionization technique in which a relatively small quantity of internal energy is supplied to the molecule [24], so that only the parent peak is detected [22,23]. From this, we can quantitatively estimate the contribution of the reaction pathways to discuss the contribution of each mechanism.

2. Experimental

2.1. Catalyst preparation

$Cs_{2.5}H_{0.5}PW_{12}O_{40}$ (abbreviated as Cs2.5) was prepared according to the literature [25,26]. An appropriate amount of the aqueous solution (0.10 mol dm^{-3}) of Cs_2CO_3 (Merck, >99%) was added dropwise at a constant rate of about 1 cm^3 min^{-1} to an aqueous solution (0.08 mol dm^{-3}, 20.0 cm^3) of $H_3PW_{12}O_{40}$ (Nippon Inorganic Color and Chemicals Co.) at room temperature under vigorous stirring. From the beginning of addition of Cs_2CO_3, very fine particles (precipitates) were formed, making the solution milky. After aging overnight at room temperature, water was slowly removed by evaporation at 323 K. The resulting white solid was ground into powder. The surface area was found to be 120 m^2 g^{-1} by the BET method.

Pt-$Cs_{2.5}H_{0.5}PW_{12}O_{40}$ (abbreviated as Pt-Cs2.5) was also prepared according to the literature [13,14]. Amount of Pt was adjusted to 1.0 wt%. An aqueous solution (0.041 mol dm^{-3}, 12.1 cm^3) of H_2PtCl_6 (Wako Pure Chemical Ind. Ltd.) was added to the aqueous solution (0.148 mol dm^{-3}, 20 cm^3) of $H_3PW_{12}O_{40}$ at room temperature. Subsequently, the aqueous solution of Cs_2CO_3 (0.108 mol dm^{-3}, 34.6 cm^3) was added to the solution under vigorous stirring, forming a milky suspension. After evacuation to remove water, the resulting solid was calcined at 573 K in air for 2 h. The surface area of Pt-Cs2.5 was 80 m^2 g^{-1}.

Sulfated zirconia (abbreviated as SZ) was prepared by the method described in the literature [11,23]. $Zr(OH)_4$ was obtained from an aqueous solution of $ZrCl_2O{\cdot}8H_2O$ (Wako Pure Chemicals Ind. Ltd.) by precipitation with an aqueous ammonia at pH = 9, and the precipitate was filtered and washed with water repeatedly until the filtrate was neutral. The obtained solid was dried at 373 K for 24 h. A total of 100 cm^3 of H_2SO_4 (1 mol dm^{-3}) was added to 9.9 g of $Zr(OH)_4$ under stirring, and the stirring was continued for 1 h. Then, the solid was filtered, dried at 373 K for 24 h, and calcined at 893 K in air for 3 h. The surface area was 90 m^2 g^{-1}. Pt-sulfated zirconia (1.0 wt.%, abbreviated as Pt-SZ) was prepared by impregnating SZ with the aqueous solution of H_2PtCl_6 (0.041 mol dm^{-3}). The obtained solid was calcined at 573 K in air for 2 h, and its surface area was 85 m^2 g^{-1}.

Tungstena–zirconia (W/Zr ratio = 0.1, abbreviated as WZ) was prepared by an impregnation method. Powder of ammonium para-tungstate $(NH_4)_{10}W_{12}O_{41}{\cdot}5H_2O$ was first added to hot water (not dissolved instantly) and then the suspension was stirred under ultrasonic radiation for 5 min to form the solution. $Zr(OH)_4$ (10 g, Daiichi Kigenso Co.) that had been dried at 373 K overnight was impregnated with an aqueous solution (0.016 mol dm^{-3}) of $(NH_4)_{10}W_{12}O_{41}{\cdot}5H_2O$ at room temperature. The solid was dried overnight at 373 K, and calcined at 1073 K in air for 3 h. Pt-WO_3/ZrO_2 (1.0 wt.%, abbreviated as Pt-WZ) was prepared by incipient-wetness impregnation using the aqueous solution of H_2PtCl_6 by the same method as employed for Pt-SZ. The obtained solid was calcined at 573 K in air for 2 h, and its surface area was 70 m^2 g^{-1}.

2.2. Materials

As a reactant, *n*-butane (Takachiho Chemical Ind. Co. Ltd., Ultra pure) was used without further purification. 1,4-$^{13}C_2$-*n*-butane (^{13}C: 99%) purchased from ISOTEC Inc. was used without further purification.

2.3. Catalytic reaction

Skeletal isomerization of *n*-butane was performed at 393–623 K in a closed circulation system (200 cm^3) made of Pyrex glass with greaseless cocks equipped with an on-line GC. After the catalyst was pretreated in vacuum at 573 K for 2 h (for Cs2.5, WZ, Pt-Cs2.5, and Pt-SZ) or at 673 K for 4 h (for SZ and Pt-SZ), 40 Torr (1 Torr = 133 Pa) of *n*-butane (or 1,4-$^{13}C_2$-*n*-butane) was introduced. In the case of Pt-promoted catalysts, 200 Torr of H_2 was also added to the reaction system. After the reaction, the reactant *n*-butane and products including isobutane and C_1–C_8 hydrocarbons

were analyzed by an on-line GC (Hitachi, Gas Chromatograph 163) with a column of VZ-7 (3 mm × 6 m). In the case of 1,4-$^{13}C_2$-*n*-butane, the reactant and product were separated and analyzed by FI-MS (JEOL JNM-ECP400) to determine ^{13}C-distribution, and by ^{13}C NMR (JEOL EX-400) to determine the ^{13}C-location in butanes.

3. Results

Fig. 1 shows the time courses of the skeletal isomerization of *n*-butane over the solid acids at 523 K. In the initial stage the reaction of *n*-butane proceeded rapidly on SZ, but after about 30 min of reaction time the reaction became slow. Among these catalysts, WZ was least active. Cs2.5 showed a moderate activity. The deactivations for WZ and Cs2.5 were only slight. The selectivities to isobutane over SZ and Cs2.5 were high in the initial stage, and decreased gradually with reaction time. In contrast, the selectivity over WZ increased with reaction time and became nearly constant after 120 min. By-products on WZ in the initial stage were C_2 and C_3 hydrocarbons. Among these catalysts, Cs2.5 showed the highest selectivity. At 180 min of the reaction time, the selectivity was in the following order: Cs2.5 > WZ > SZ.

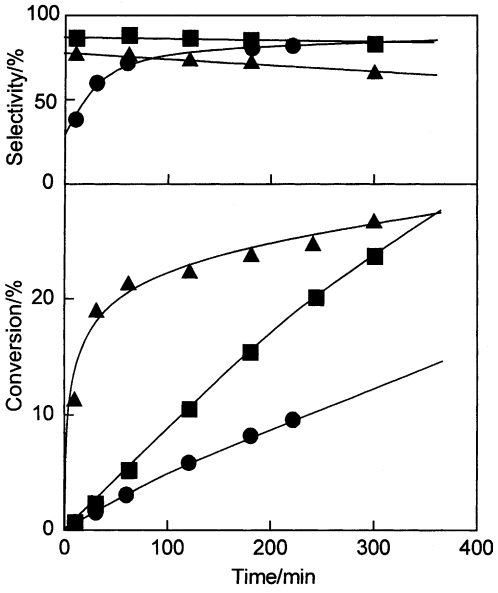

Fig. 1. Time courses of skeletal isomerization of *n*-butane over typical solid acids at 523 K. (■) $Cs_{2.5}H_{0.5}PW_{12}O_{40}$, (▲) sulfated ZrO_2, and (●) WO_3/ZrO_2. Reaction conditions: *n*-butane 40 Torr; catalyst weight 0.5, 0.5, and 2.0 g for $Cs_{2.5}H_{0.5}PW_{12}O_{40}$, sulfated ZrO_2, and WO_3/ZrO_2, respectively.

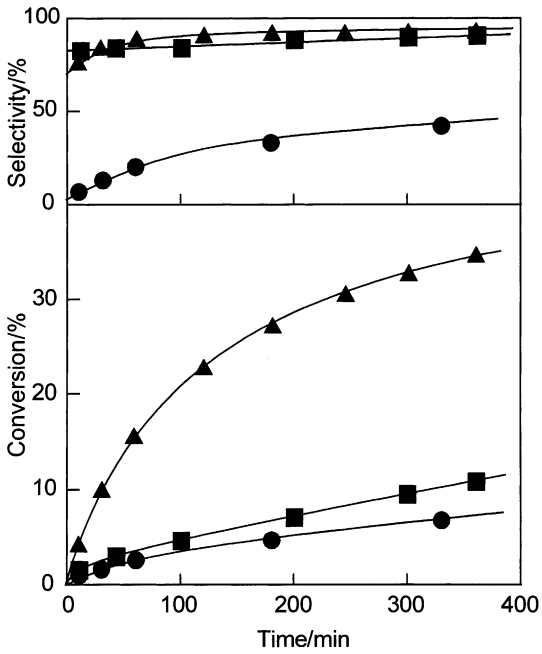

Fig. 2. Time courses of skeletal isomerization of *n*-butane over Pt-promoted catalysts in the presence of H_2 at 523 K. (■) Pt-$Cs_{2.5}H_{0.5}PW_{12}O_{40}$, (▲) Pt-sulfated ZrO_2, and (●) Pt-WO_3/ZrO_2. Reaction conditions: *n*-butane 40 Torr; H_2 200 Torr; catalyst weight 0.2, 0.05, and 0.5 g for Pt-$Cs_{2.5}H_{0.5}PW_{12}O_{40}$, Pt-sulfated ZrO_2, and Pt-WO_3/ZrO_2, respectively.

Fig. 2 presents the time courses of the skeletal isomerization of *n*-butane over Pt-promoted catalysts in the presence of H_2 at 523 K. Pt-SZ was highly active, but considerable deactivation was observed. The conversions for Pt-Cs2.5 and Pt-WZ increased linearly with reaction time, indicating little deactivation. Pt-SZ and Pt-Cs2.5 showed high selectivities to isobutane (>90% at 300 min). The selectivity for Pt-WZ was low because of formation of C_1–C_3 hydrocarbons by the hydrogenolysis reaction.

Table 1 summarizes the catalytic activities and selectivities for the skeletal isomerization of *n*-butane. Comparison

Table 1
Catalytic activity and selectivity for skeletal isomerization of *n*-butane[a]

Catalyst	Rate (μmol g^{-1} h^{-1})	C_1–C_2	Selectivity (mol%)			
			C_3	*iso*-C_4	C_5	C_6–C_8
WO_3/ZrO_2	8.1	4.0	8.7	83.2	4.1	0.0
$Cs_{2.5}H_{0.5}PW_{12}O_{40}$	64.5	0.4	6.8	87.1	5.7	0.0
SO_4^{2-}/ZrO_2	752.5	0.2	13.8	78.3	7.7	0.0
Pt-WO_3/ZrO_2	14.1	29.7	20.2	49.5	0.6	0.0
Pt-$Cs_{2.5}H_{0.5}PW_{12}O_{40}$	57.9	2.2	3.6	92.0	2.2	0.0
Pt-SO_4^{2-}/ZrO_2	2523.6	7.0	7.9	84.4	0.7	0.0

[a] The reaction was performed at 523 K with *n*-butane 40 Torr. H_2 200 Torr was added over Pt-promoted catalysts. The data was taken at about 10% conversion.

at ca.10% of the conversion at 523 K shows that the reaction rate was higher over the Pt-promoted catalysts than over the unpromoted catalysts, except for Cs2.5. With regard to selectivity, Pt-promoted catalysts other than Pt-WZ are more selective than the unpromoted solid acids. Pt-WZ yielded large amounts of C_1–C_3 alkanes as by-products, because of the hydrogenolysis reaction. In the case of the solid acids, C_3 and C_5 hydrocarbons were formed as by-products (Table 1), indicating that dimerization-cracking (bimolecular mechanism) proceeded over these catalysts, as will be discussed below. In contrast, the C_5 hydrocarbons were formed very little on Pt-SZ and Pt-Cs2.5.

Fig. 3 shows the isotopic distributions of *n*-butane and isobutane over Cs2.5 and WZ. Binomial patterns of ^{13}C-isobutane (open rectangles in Fig. 3) were calculated from the content ratio (r) of ^{13}C to ^{12}C, assuming binomial distribution, $1{:}4r{:}6r^2{:}4r^3{:}r^4$, where r was determined by optimization between the observed and calculated fractions for $x = 0, 1, 3, 4$ in $^{13}C_x{}^{12}C_{4-x}H_{10}$ of isobutane [22,23]. For both catalysts, *n*-butane mainly consisted of $^{13}C_2$-*n*-butane (Fig. 3a). The isotopic distributions of isobutane at 423 K on both catalysts were very close to the binomial distributions (Fig. 3b). This shows that the isomerization over these catalysts at 423 K proceeds via an intermolecular process and that the rearrangement is rapid, which accords with the previous results for SZ [22]. In contrast, at 523 K both the catalysts yielded mainly $^{13}C_2$-isobutane (Fig. 3c), whose fractions were much greater than those of the binomial ones. The patterns shown in Fig. 3c demonstrate that the isomerization proceeds through both the competitive pathways, intermolecular and intramolecular.

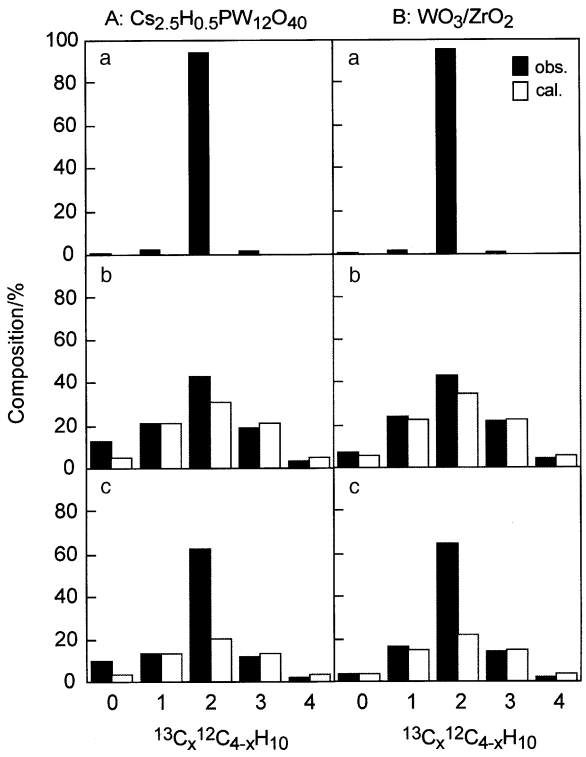

Fig. 3. ^{13}C-distribution of *n*-butane and isobutane in the isomerization of 1,4-$^{13}C_2$-*n*-butane over (A) $Cs_{2.5}H_{0.5}PW_{12}O_{40}$ and (B) WO_3/ZrO_2. (a) *n*-Butane at 423 K, (b) isobutane at 423 K, and (c) isobutane at 523 K. The conversions were around 10%.

Table 2 summarizes the isotopic distributions of isobutane and *n*-butane. Table 2 also shows the ratios of observed fraction of $^{13}C_2$-isobutane to the calculated fraction. These ratios were close to unity (1.3 for Cs2.5 and 1.3 for WZ) at 423 K, and were nearly independent of the conversions, e.g., 1.3 and 1.5 at the conversions of 11.0 and 27.5%, respectively, on Cs2.5.

In Fig. 4, the contribution of intramolecular pathway (monomolecular mechanism) on these solid acids is plotted against the reaction temperature. The contribution of the monomolecular pathway was estimated from the amounts by which the $^{13}C_2$-isobutane fraction exceeded that of the calculated binomial distribution [22,23]. At low temperatures, the contributions of the monomolecular pathway were very low (less than 12%) for all solid acids. A noteworthy finding is that the contributions of monomolecular pathway showed similar trends; that is, they increased with increasing temperature. Within these temperature ranges, the contributions of the monomolecular pathway were still less than 50%.

Table 2
Selected values of observed isotopic distributions of isobutane and *n*-butane in the reaction of 1,4-$^{13}C_2$-*n*-butane[a]

Catalyst	Temperature (K)	Conversion (%)	Isobutane (%)					*n*-Butane (%)				
			$^{13}C_0$	$^{13}C_1$	$^{13}C_2$	$^{13}C_3$	$^{13}C_4$	$^{13}C_0$	$^{13}C_1$	$^{13}C_2$	$^{13}C_3$	$^{13}C_4$
$Cs_{2.5}H_{0.5}PW_{12}O_{40}$	423	11.0	13.0	21.9	41.9 (1.3)	19.3	3.9	0.7	2.8	94.3	2.2	0.0
	423	27.5	5.8	22.7	46.9 (1.5)	20.1	4.5	1.5	5.0	89.7	3.2	0.6
	523	12.8	6.6	13.8	62.6 (3.1)	14.9	2.1	1.8	2.9	93.1	2.1	0.1
WO_3/ZrO_2	423	10.2	6.8	23.7	43.2 (1.3)	22.0	4.3	0.6	2.3	95.7	1.4	0.0
Pt-$Cs_{2.5}H_{0.5}PW_{12}O_{40}$	423	10.1	2.8	4.3	90.6 (17.8)	2.1	0.2	1.7	2.5	93.7	2.1	0.0

Values in parentheses are the ratios of the observed fractions of $^{13}C_2$ isobutane to the calculated fractions.

[a] Reaction conditions; *n*-butane 40 Torr. H_2 200 Torr was added over Pt-$Cs_{2.5}H_{0.5}PW_{12}O_{40}$. Isotopic distributions were estimated with field-ionization mass spectrometry.

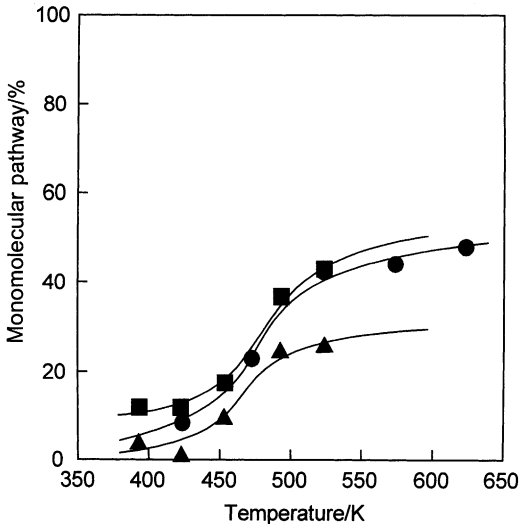

Fig. 4. Contribution of the monomolecular pathway in skeletal isomerization of *n*-butane over solid acids. (■) $Cs_{2.5}H_{0.5}PW_{12}O_{40}$, (▲) sulfated ZrO_2, and (●) WO_3/ZrO_2.

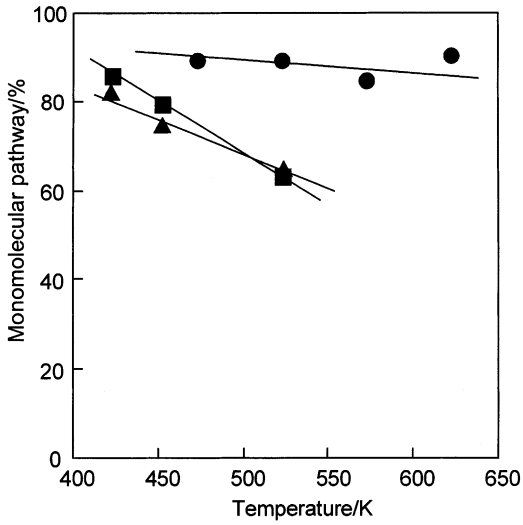

Fig. 6. Contribution of the monomolecular pathway in skeletal isomerization of *n*-butane over Pt-promoted catalysts. (■) Pt-$Cs_{2.5}H_{0.5}PW_{12}O_{40}$, (▲) Pt-sulfated ZrO_2, and (●) Pt-WO_3/ZrO_2.

Fig. 5 shows the isotopic distributions of *n*-butane and isobutane over Pt-Cs2.5 and Pt-WZ. It was confirmed that *n*-butane consisted mainly of $^{13}C_2$-butane over both the catalysts (Fig. 5a). The isotopic distributions of isobutane

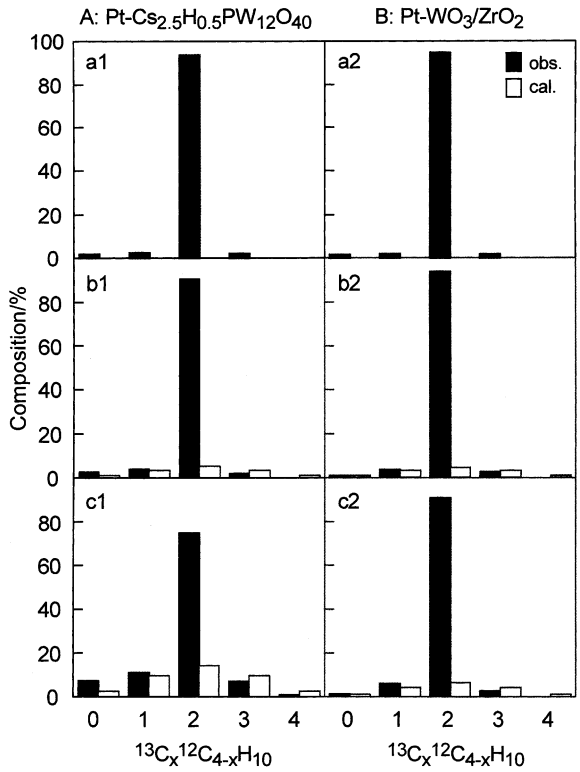

Fig. 5. ^{13}C-distribution of *n*-butane and isobutane in the isomerization of 1,4-$^{13}C_2$-*n*-butane over (A) Pt-$Cs_{2.5}H_{0.5}PW_{12}O_{40}$ and (B) Pt-WO_3/ZrO_2. (a1) *n*-Butane at 423 K, (a2) *n*-butane at 473 K, (b1) isobutane at 423 K, (b2) isobutane at 473 K, (c1) isobutane at 523 K, and (c2) isobutane at 573 K. The conversions were about 10%.

were quite different from the binomial distributions; the fractions of $^{13}C_2$-butane were much greater than those of the binomial distributions. These patterns indicate that the isomerization on Pt-promoted catalysts proceeds through the intramolecular pathway (the monomolecular mechanism).

In Fig. 6, the contribution of the monomolecular mechanism over Pt-promoted catalyst is plotted against reaction temperature. In contrast to the results on the solid acids (Fig. 4), the contributions of monomolecular mechanism were high at these temperatures over all the Pt-promoted catalysts. Especially, the contributions exceeded 80% at low temperature. Contrary to the trend in Fig. 4, the contributions tended to decrease with increasing temperature.

Fig. 7 shows the effects of hydrogen pressure on the contribution of the bimolecular mechanism, selectivity to C_5 hydrocarbons, and rates of isomerization and hydrogenolysis on Pt-WZ at 473 K. As is clear from the figure, the changes in the contribution of bimolecular pathways and the selectivity to C_5 hydrocarbons are similar. As hydrogen pressure increased, the rate for the isomerization decreased and that for the hydrogenolysis increased.

In order to determine the location of ^{13}C in *n*-butane after the reaction, the ^{13}C NMR was measured. Before the reaction, a single peak at 13.8 ppm (methyl carbon) was detected. In contrast, after the reaction (conversion of *n*-butane = 12.4%) over Cs2.5 at 423 K, a new peak at 24.9 ppm (methylene carbon) was observed, in addition to the peak at 13.8 ppm. The relative peak intensities for methyl and methylene carbon were 94.3 and 5.7%, respectively. When *n*-butane containing ^{13}C in natural abundance was measured, the two peaks were detected with almost the same intensity, indicating similar sensitivities of carbon atoms for the NMR measurement.

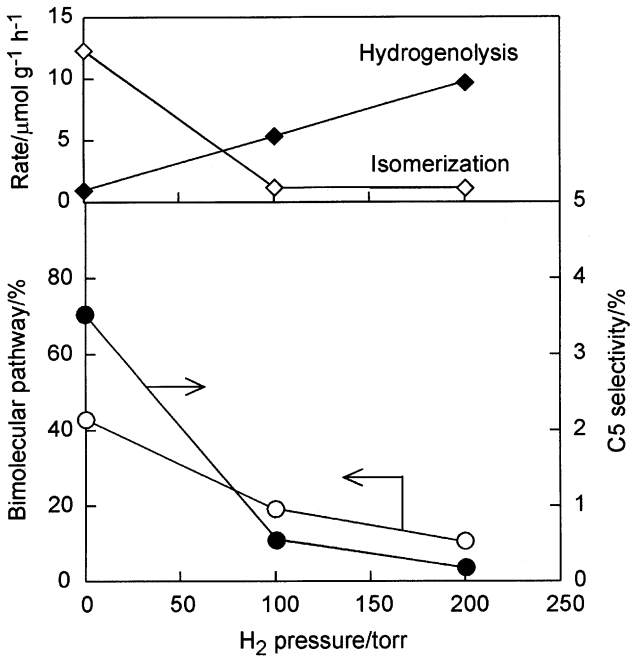

Fig. 7. Effects of H_2 pressure on (○) contribution of the bimolecular pathway, (●) selectivity to C5 hydrocarbons, and rate of (◇) isomerization, and (◆) hydrogenolysis on Pt-WO_3/ZrO_2 at 473 K.

The amounts of $^{13}C_2$-isobutane and 1,3-$^{13}C_2$-*n*-butane produced were determined from FI-MS of isobutane and ^{13}C NMR of *n*-butane, respectively. The data for about 10% conversion were used. In Fig. 8, the ratio of rate constants (k_c: carbon-shift reaction and k_s: skeletal isomerization in Scheme 1A) for Cs2.5 is plotted against the reaction temperature. This ratio corresponds to that of the amount of 1,3-$^{13}C_2$-*n*-butane to $^{13}C_2$-isobutane formed from the monomolecular pathway. As shown in Fig. 8, this ratio is about 10 at 393 K but decreases greatly with increasing temperature, reaching about 0.7 at 523 K on Cs2.5.

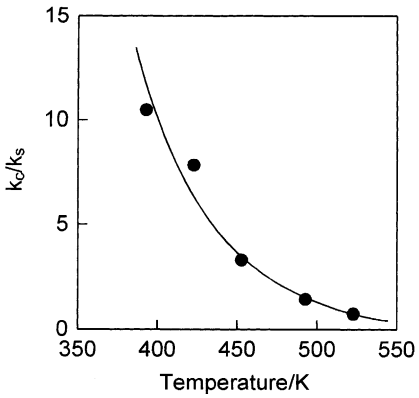

Fig. 8. Ratio of the amount of 1,3-$^{13}C_2$-*n*-butane to that of $^{13}C_2$-isobutane over $Cs_{2.5}H_{0.5}PW_{12}O_{40}$. The amounts of 1,3-$^{13}C_2$-*n*-butane and $^{13}C_2$-isobutane were estimated from FI-MS of isobutane and ^{13}C NMR of *n*-butane, respectively. The conversions were about 10%.

4. Discussion

4.1. Proposed reaction mechanism

The possible rearrangement patterns of ^{13}C in the isomerization when 1,4-$^{13}C_2$-*n*-butane is used as reactant are summarized in Scheme 1. In the monomolecular mechanism, the isomerization would involve a protonated methylcyclopropane and a sequent primary carbenium ion as intermediates. If the reaction proceeds through the monomolecular mechanism, $^{13}C_2$-isobutane in the topoisomers of isobutane would be produced exclusively (intramolecular rearrangement), together with 1,3-$^{13}C_2$-*n*-butane as an isotopomer by self-isomerization, when $^{13}CH_3$–$(CH_2)_2$–$^{13}CH_3$ was used as a reactant (Scheme 1A). Since the cracking of secondary carbenium ion directly to C_1–C_3 hydrocarbons is unfavorable from the viewpoint of energy [17], the selectivity to isobutane will be 100% in this mechanism. On the other hand, the bimolecular mechanism (Scheme 1B) is possible if butenes and *sec*-butyl carbenium ion are formed on the catalyst surface to form octyl cation [17]. The β-scission of octyl cation would yield C_4 moieties, together with the by-products of C_3 and C_5 alkanes. In this case, intermolecular isotopic scrambling in product isobutane is expected, as shown in Scheme 1B.

4.2. Skeletal isomerization of n-butane over solid acids

In the skeletal isomerization of *n*-butane over solid acids, one of the critical steps is activation of *n*-butane to *sec*-carbenium ion. Two processes are possible, that is, protonation of *n*-butane, and dehydrogenation ((1) in Scheme 2) or hydride abstraction by Lewis acid ((2) in Scheme 2). These two steps are supposed to require high acid strength for the acidic sites. Although the subsequent reaction pathways such as the rearrangement of carbenium ions and the hydride transfer reaction to form isobutane are also proposed to be the critical steps [13], in any event, the acid strength must sensitively influence the catalytic activity. The order of the initial activity, SZ > Cs2.5 > WZ (Table 1), can be explained by the acid strengths of these solid acids. TPD of NH_3 showed that the acid strength of these catalysts was in the order of SZ > Cs2.5 > WZ [27,28] and that the acid amount was similar [25,28].

The selectivity over solid acids is expected to be closely related to the reaction mechanism. As was explained above, the bimolecular pathway would readily cause the cracking reaction, whereas the isomerization reaction would selectively proceed under the monomolecular pathway. Fig. 4 clearly demonstrates that the reaction took place via similar pathways over all these solid acids, that is, the bimolecular pathway at low temperatures and parallel pathways (mono and bimolecular pathways) at high temperatures. In conformity with this, the by-products were C_3 and C_5 hydrocarbons (Table 1). As is well known, the bimolecular

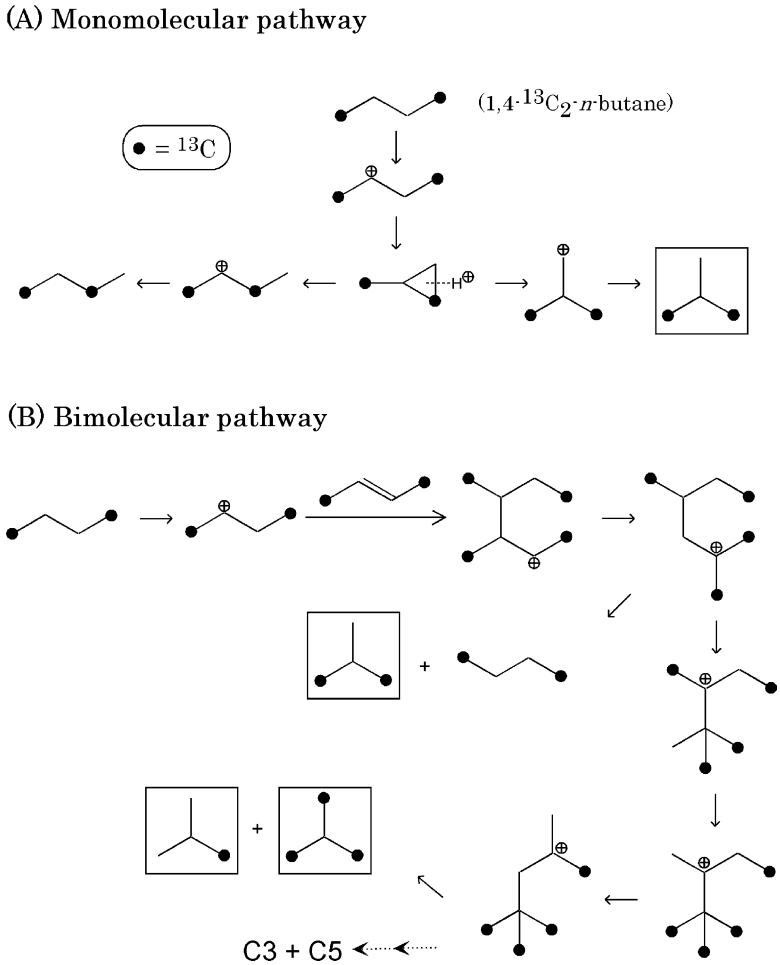

Scheme 1. (A) Monomolecular pathway. (B) Bimolecular pathway.

pathway is favorable from the viewpoint of energy, because this pathway proceeds via *sec*-carbenium ion. On the other hand, the monomolecular pathway must path through a primary carbenium ion intermediate (Scheme 1). Therefore, a reasonable conclusion is that the bimolecular pathway was preferential at low temperatures over all these solid acids. The increased contribution of monomolecular pathway with increasing reaction temperature can be explained by the large activation energy for the monomolecular pathway [17]. An intriguing finding is that the contribution of the reaction pathway was essentially the same for these solid acids, although acid strength differed greatly [27].

4.3. Skeletal isomerization of Pt-promoted catalysts

Over the bifunctional catalysts (metal-promoted solid acids), the bifunctional mechanism has been proposed [29,30]. In this mechanism, first, *n*-butane is dehydrogenated to butenes ((4) in Scheme 3), and then, the butenes are protonated on acidic sites to form *sec*-carbenium ion ((5) in Scheme 3). The steps represented in (4) in Scheme 3 are in equilibrium. These steps are supported by the follow-

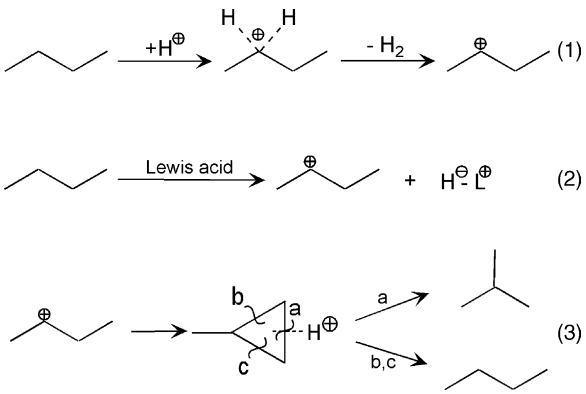

Scheme 2.

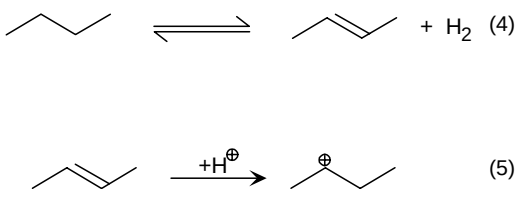

Scheme 3.

ing: (1) the reaction rate is independent of the Pt content, and (2) the rate is inversely dependent on the hydrogen pressure (Fig. 7) [13].

In the bifunctional mechanism, the activation of *n*-butane is expected to be easier than in the acidic mechanism ((1) and (2) in Scheme 2). Higher reaction rates were obtained for the bifunctional catalysts (Table 1), which is probably due to the bifunctional mechanism.

In the presence of H_2 over the bifunctional catalysts, the content of alkenes would be greatly suppressed, which is unfavorable for the bimolecular mechanism. Consistent with the above idea, the reaction over these bifunctional catalysts proceeded exclusively via the monomolecular pathway (Fig. 6). As the reaction temperature increased, the contribution of the bimolecular mechanism increased. This is probably due to the increase in the equilibrium concentrations of butenes.

As shown in Fig. 7, the contribution of bimolecular pathway and the selectivity to C_5 hydrocarbons changed similarly to the hydrogen pressure over Pt-WZ. This result is consistent with the expectation from Scheme 1.

4.4. Rearrangement of carbon atom in protonated cyclopropane intermediate

In the monomolecular mechanism for *n*-butane isomerization, protonated methylcyclopropane intermediate has been proposed [17]. The skeletal isomerization will be brought about by the cleavage of the bond "a" in (3) in Scheme 2. On the other hand, the cleavages of the other bonds, "b" and "c" in (3) in Scheme 2, will cause the shift of carbon, giving back to *n*-butane. The former must pass through a primary carbenium ion, whereas the latter can pass through the protonated methylcyclopropane *sec*-carbenium ions (in Scheme 1A). The energy levels of these ions are in the order of *sec*-carbenium ion > protonated methyl cyclopropane > primary carbenium ion [17]. As a matter of fact, the carbon-shift reaction took place more rapidly than the skeletal isomerization of *n*-butane over H_2SO_4 [17], which supports the above mechanism.

As shown in Fig. 8, the carbon-shift reaction proceeded more than 10 times as fast as the skeletal isomerization over Cs2.5 at 423 K, which is consistent with the result over H_2SO_4. However, at 523 K, the ratio in reaction rates decreased to about 0.7. The difference in activation energy between the protonated methylcyclopropane and *sec*-carbenium ions obtained for Cs2.5 was estimated to be 13.2 kJ mol^{-1}, which is much smaller than that for H_2SO_4 (60 kJ mol^{-1}) [17]. This difference may be brought about by the stabilization of ions through the adsorption on the catalyst surface. Furthermore, about the fact that the skeletal isomerization was slightly more rapid than the carbon-shift reaction at 523 K, we speculate that the methylcyclopropane intermediate orients specially in the manner of end-on [31] shown in Fig. 9, which make the cleavage of the bond "a" in (3) in Scheme 2 easier.

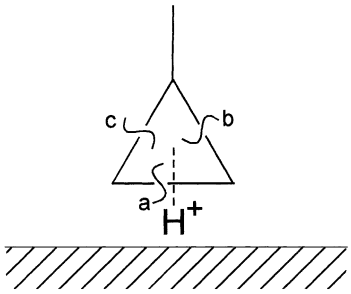

Fig. 9. Proposed model of the methyl cyclopropane intermediate on the surface of the catalyst.

5. Conclusion

The reaction mechanism of the skeletal isomerization of *n*-butane over solid acids such as $Cs_{2.5}H_{0.5}PW_{12}O_{40}$, sulfated ZrO_2, and WO_3/ZrO_2 and their Pt-promoted catalysts were investigated by using 1,4-$^{13}C_2$-*n*-butane as reactant. The reaction took place via similar pathways independently of the kind of solid acids, that is, via a bimolecular pathway at low temperatures and via parallel (mono and bimolecular) pathways at high temperatures. On the other hand, the monomolecular mechanism operated mainly the isomerization reaction over Pt-promoted catalysts over the wide range of the reaction temperature.

Acknowledgements

This work was partially supported by Core Research for Evolutional Science and Technology (CREST) of Japan Science and Technology Corporation (JST).

References

[1] G.A. Olah, G.K.S. Parakash, J. Sommer, Superacids, Wiley/Interscience, New York, 1985.
[2] G.A. Olah, O. Farooq, A. Husain, N. Ding, N.J. Trivedi, J.A. Olah, Catal. Lett. 10 (1991) 239.
[3] H. Hino, K. Arata, J. Am. Chem. Soc. 101 (1979) 6439.
[4] K.T. Wan, C.B. Khouw, M.E. Davis, J. Catal. 158 (1996) 311.
[5] C.-Y. Hsn, C.R. Heimbuch, C.T. Armes, B.C. Gates, J. Chem. Soc., Chem. Commun. (1992) 1645.
[6] K. Na, T. Okuhara, M. Misono, J. Chem. Soc., Faraday Trans. 1 91 (1995) 367.
[7] N. Essayem, G. Coudurier, M. Fournier, J.C. Vedrine, Catal. Lett. 34 (1995) 223.
[8] M. Hino, K. Arata, J. Chem. Soc., Chem. Commun. (1987) 1259.
[9] J.C. Yori, C.L. Pieck, J.M. Parera, Appl. Catal. A 181 (1999) 5.
[10] M. Hino, K. Arata, Catal. Lett. 30 (1995) 25.
[11] K. Ebitani, J. Konishi, H. Hattori, J. Catal. 131 (1991) 257.
[12] N.A. Cusher, Handbook of Petroleum Refining Process, McGraw-Hill, New York, 1996.
[13] K. Na, T. Okuhara, M. Misono, J. Catal. 170 (1997) 96.
[14] T. Okuhara, T. Yamada, K. Seki, K. Johkan, T. Nakato, Micropor. Mesopor. Mater. 21 (1998) 637.
[15] J.C. Yori, J.M. Parera, Catal. Lett. 65 (2000) 205.

[16] S. Eibl, R.E. Jentoft, B.C. Gates, H. Knözinger, Phys. Chem. Chem. Phys. 2 (2000) 2565.
[17] B.C. Gates, Catalytic Chemistry, Wiley, New York, 1992.
[18] F. Grain, L. Seyfried, P. Girard, G. Marie, A. Abdulsamad, J. Sommer, J. Catal. 151 (1995) 26.
[19] V. Adeeva, G.D. Lei, W.M.H. Sachtler, Catal. Lett. 33 (1995) 135.
[20] C. Bearez, F. Avendano, F. Chevalier, M. Guisnet, Bull. Soc. Chim. Fr. 3 (1985) 346.
[21] H. Matsuhashi, H. Shibata, H. Nakamura, K. Arata, Appl. Catal. A 187 (1999) 99.
[22] T. Suzuki, T. Okuhara, Chem. Lett. (2000) 470.
[23] T. Suzuki, T. Okuhara, Catal. Lett. 72 (2001) 111.
[24] G.A. St. John, S.E. Buttrill Jr., M. Anbar, Organic chemistry of coal, in: J.W. Larsen (Ed.), ACS Symposium Series 71, American Chemical Society, Washington, DC, 1978, pp. 223–239.
[25] T. Okuhara, T. Nishimura, H. Watanabe, M. Misono, J. Mol. Catal. 74 (1992) 247.
[26] S. Tatematsu, T. Hibi, T. Okuhara, M. Misono, Chem. Lett. (1984) 865.
[27] T. Okuhara, T. Nishimura, M. Misono, Stud. Surf. Sci. Catal. 101 (1996) 581.
[28] L. Li, Y. Yoshinaga, T. Okuhara, Phys. Chem. Chem. Phys. 1 (1999) 4913.
[29] G.L. Frischkorn, P.J. Kuchar, R.K. Olson, Energy Prog. 8 (1988) 154.
[30] B.C. Gates, J.R. Katzer, G.C. Schuit, Chemistry of Catalytic Processes, McGraw-Hill, New York, 1979.
[31] F. Chevalier, M. Guisnet, R. Maurel, in: G.C. Bond, P.B. Wells, F.C. Tompkins (Eds.), Proceedings of the 6th International Congress on Catalysts, London, 1976, p. 478.